Construction and Building Materials 342 (2022) 128034

Contents lists available at ScienceDirect

Construction and Building Materials

journal homepage: www.elsevier.com/locate/conbuildmat

Performance evaluation of electro-mechanical impedance based state of health estimation of sacrificial anodes in reinforced concrete structures

Durgesh Tamhane [a], Jeslin Thalapil [a], Sauvik Banerjee [b], Siddharth Tallur [a,*]

[a] Department of Electrical Engineering, Indian Institute of Technology Bombay, Mumbai, 400076, Maharashtra, India
[b] Department of Civil Engineering, Indian Institute of Technology Bombay, Mumbai, 400076, Maharashtra, India

ARTICLE INFO

Keywords:
Cathodic protection system
Corrosion monitoring
Electro-mechanical impedance (EMI)
Sacrificial anode
Smart infrastructure
Structural health monitoring
Reinforced concrete

ABSTRACT

Sacrificial anodes have been commonly used as a convenient and an affordable method to protect steel rebars embedded in reinforced concrete structures from corrosion, thereby extending their remaining service life. While the electro-mechanical impedance (EMI) technique has been established to be an effective technique for monitoring of concrete properties and corrosion, the effectiveness of this technique when applied to estimating state-of-health of sacrificial anodes embedded in concrete has not yet been investigated. In this work, we study the performance of EMI-based monitoring of incipient corrosion of sacrificial anodes embedded in conductive mortar and reinforced concrete. Through impressed current based accelerated corrosion experiments, we demonstrate that the root mean square deviation (RMSD) of the conductance spectra of lead zirconate titanate (PZT) transducer fitted to a sacrificial anode provides high sensitivity as a performance metric to analyze change in state-of-health of the anode. Further, analytical and FE models are developed for validating the experimental results obtained using impressed current based accelerated corrosion setup. It is found that the RMSD varies non-linearly with increasing time of application of impressed current, that can be explained adequately by the delamination dynamics of corrosion by-products and damping captured by the models. The primary advantage of this technique over conventional methods is that the degradation of the sacrificial anode in the concrete structure can be non-destructively and deterministically assessed in real time.

1. Introduction

Reinforced concrete is widely used in civil engineering structures like buildings, dams, bridges, etc. While the reinforcement (steel) bars are susceptible to corrosion, well-compacted and precisely manufactured concrete mix has high alkalinity, low permeability and high resistivity, making it a durable protection against corrosion [1]. However, in practice such a perfect concrete mix is rarely achieved and the reinforcements are vulnerable to corrosion. The initiation of corrosion of the reinforcements embedded in concrete usually begins as the concrete deteriorates due to severe environmental conditions or due to seepage of corrosive agents owing to poor quality of preparation. After corrosion initiation, the service life of the structure begins to deteriorate, eventually leading to premature failure. The global economic burden for repair and maintenance of corroded structures is estimated to be upwards of USD$2.5 trillion [2]. One of the traditional methods for prevention of corrosion of reinforcement bars is by installing a cathodic protection system [3,4], that operates based on the difference in the electrochemical activity of metals. A metal with higher electrochemical activity on the galvanic scale tends to corrode more preferentially than a metal with lower electrochemical activity when electrically connected in the same environment, and thus provides protection against corrosion to the latter. This type of protection is called passive cathodic protection, and the metal with higher electrochemical activity is called a sacrificial anode. In passive cathodic protection system, the sacrificial anode is consumed over time due to corrosion, the rate of which is dependent on the nature of the corrosive environment of the infrastructure, and the protection expires beyond the life-time of the sacrificial anode. Thus, it is necessary to actively monitor the efficacy and lifetime of the installed sacrificial anodes in order to prolong the service-life of the structure under protection [5,6].

Conventional nondestructive testing (NDT) methods for monitoring cathodic protection systems include half-cell potential measurement [25], open-circuit potential test [26], DC current density measurement [27] and zero resistance ammeter (ZRA) measurement [28]. Some of these measurements require fragile three-electrode apparatus, while others require the disconnection of the cathodic system and are thus not amenable to real-time monitoring. The ZRA measurement technique involves significant overhead due to the requirement of

* Corresponding author.
E-mail addresses: dtamhane@iitb.ac.in (D. Tamhane), stallur@ee.iitb.ac.in (S. Tallur).

https://doi.org/10.1016/j.conbuildmat.2022.128034
Received 10 September 2021; Received in revised form 25 May 2022; Accepted 31 May 2022
Available online 11 June 2022

Table 1
Overview of application of PZT transducers and EMI for evaluation of concrete structures and corrosion.

Reference	Application
Monitoring of concrete properties	
Zhang et al. [7]	Early age hydration and setting of cement paste with embedded piezoelectric transducers.
Su et al. [8]	Stiffness development and compressive strength gain at very early age of cementitious materials.
Negi et al. [9]	Effect of orientation of PZT patches on monitoring concrete hydration of RC beams.
Zhao et al. [10]	Concrete damage induced by compression evaluated by a spherical smart aggregate sensor.
Ai et al. [11]	Comparison of surface and embedded PZT sensors for structural impact damage on concrete.
Saravanan et al. [12]	Smart aggregates embedded in concrete to monitor progressive strength loss under compressive loads.
Narayanan et al. [13]	Evaluation of stress and induced damage in concrete due to compressive loading.
Corrosion monitoring	
Ahmadi et al. [14]	Assessment of corrosion rate, direction and initiation in reinforced concrete.
Bansal et al. [15]	Deterioration of stiffness, mass and damping due to corrosion in prestressed concrete (PC) structures.
Shi et al. [16]	Corrosion process of reinforcement bars in concrete.
Simmers et al. [17]	Damage induced in plates and beams due to corrosion.
Park et al. [18]	Corrosion detection in 6063 T5 aluminum alloy beam using an impedance measuring chip (AD5933).
Bedekar et al. [19]	Early stage corrosion damage detection in Al-6061 alloy.
Yang et al. [20]	Monitoring local corrosion of steel beam in a simulated marine environment.
Talakokula et al. [21]	Diagnosing chloride-induced corrosion for reinforced concrete structures with embedded PZT transducers.
Talakokula et al. [22]	Detecting the onset and quantifying the level of carbonation induced rebar corrosion.
Na et al. [23]	Wall thinning effect of metal pipelines due to corrosion.
Li et al. [24]	Monitoring corrosion induced thickness loss of smart corrosion coupons embedded in concrete.

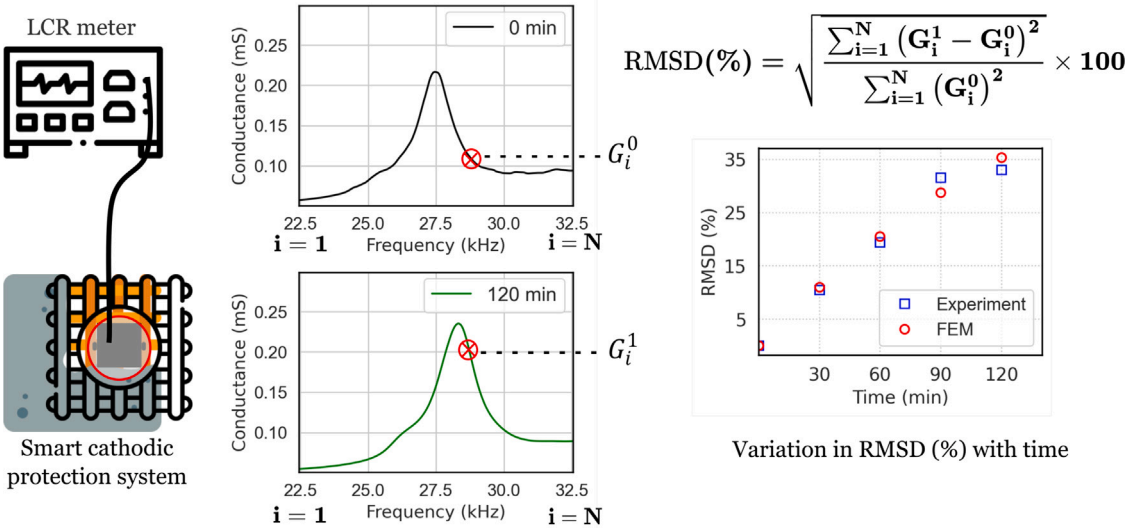

Fig. 1. Illustration of method of calculating RMSD of conductance spectra of sacrificial anode instrumented with PZT. The anode is subjected to accelerated corrosion by applying impressed current, and the variation in RMSD with increasing time of application of current is studied. The experimental results obtained in this work are also benchmarked against analytical model and finite element method (FEM).

permanently deployed data acquisition systems with necessary power supply for prolonged monitoring of the corrosion current [28]. Recently, there have been several reports of research in NDT pertaining to the use of piezoelectric sensors made of lead zirconate titanate (PZT) for structural health monitoring. Among these techniques, electro-mechanical impedance (EMI) method has received much attention due to its ability to assess local incipient damage, low-cost, high-sensitivity, fast response, easy installation and real-time detection. One of the earliest demonstrations of sensing based on EMI was reported by Liang et al. [29], where they showed the relationship of electrical impedance of the PZT and mechanical impedance of the host structure. Subsequently, several researchers have used EMI as a tool for assessment of structural damage. Soh and Bhalla [30] demonstrated the use of EMI technique for identification of concrete strength. Naidu et al. [31,32] demonstrated the capability of the EMI method to detect incipient damage in concrete structures. Subsequently, several applications of PZT transducers and EMI method for investigation of concrete properties and monitoring corrosion have been demonstrated [7–24], as summarized in Table 1.

We recently demonstrated application of EMI technique for direct in-situ measurement of the extent of degradation (corrosion) of a zinc sacrificial anode immersed in a liquid electrolyte (salt solution), supported with analytical and finite element (FE) modeling for correlating the shift in the electro-mechanical resonance frequency to the extent of corrosion [33]. While the technique is directly applicable to sacrificial anodes exposed to liquid, e.g. in marine infrastructure, the effectiveness of this technique when applied to sacrificial anodes embedded in concrete (for protection of reinforced concrete (RC) structures) has not yet been investigated. Moreover, the solid concrete cover will add significant damping to the electro-mechanical resonance, and it becomes increasingly difficult to precisely track the resonant frequency of a resonator with a low mechanical quality factor [34] without resorting to post-processing using models such as modified Butterworth Van Dyke (MBVD), as often encountered in the analysis of microelectro-mechanical systems (MEMS) [35,36]. However, the damage could potentially be quantified by measuring changes in the impedance spectrum based on the root mean square deviation (RMSD) [13]. In this work, we evaluate the performance of this method for monitoring incipient corrosion of sacrificial anodes that are embedded in conductive mortar and reinforced concrete. Impressed current based accelerated corrosion apparatus is use to corrode the

sacrificial anode and the variation in the impedance of the attached PZT transducer is observed and quantified by studying the change in RMSD of the impedance spectrum. We observe that the RMSD gradually increases with increasing time for which the impressed current is applied. The results are supported by FE simulations and analytical models developed in this work, that account for the accumulation and delamination of the corrosion products formed on the surface of the sacrificial anode embedded in concrete. We present a methodology for equivalent 2D axisymmetric analysis of the experimental specimens, and a detailed parametric study of the damping in the structure using perfectly matched layer (PML) analysis in FE simulations. The models developed in this work show excellent agreement with experimental results obtained on a sacrificial anode embedded in conductive mortar and reinforced concrete.

2. Principle of operation

The operating principle of a piezoelectric transducers such as PZT is described in detail in [37]. Owing to the converse and direct effect of piezoelectric materials, the EMI technique is based on monitoring the variation in the admittance spectra of the PZT transducer. A single PZT transducer that functions both as an actuator and a sensor can be embedded or attached to the structure that has to be monitored. As an actuator, the PZT transducer is electrically excited at high frequencies spanning a mechanical resonance of the host structure, imparting a harmonic force to the host structure. This results in a resonant response from the host structure, dependent on its structural properties, measured by the electro-mechanical impedance of the PZT transducer. Thus any change in the mechanical properties (e.g. mass loss, change in geometry) of the host structure due to corrosion results in change in the electromagnetic impedance signature. To analyze the impedance spectra and to infer the amount of degradation caused in the host structure by corrosion, the root mean square deviation of the spectrum is used as damage index. RMSD of the EMI signature has been shown to be a reliable indicator of change in concrete parameters. Tawie et al. [38] and Ghafari et al. [39] validated the feasibility of the RMSD index for the evaluation of concrete and mortar properties. Moreover, Talakokula et al. [21] have demonstrated that the RMSD can also be applied as a damage index for detecting corrosion of rebars embedded in concrete. RMSD (%) is expressed as [9,40]:

$$\text{RMSD (\%)} = \sqrt{\frac{\sum_{i=1}^{N}\left(G_i^1 - G_i^0\right)^2}{\sum_{i=1}^{N}\left(G_i^0\right)^2}} \times 100 \tag{1}$$

where G_i^0 is the baseline conductance value and G_i^1 is the post corrosion conductance value at frequency index i, corresponding to N frequency points in a given frequency range $[f_{start}, f_{end}]$, where f_{start} corresponds to index $i = 1$ and f_{end} corresponds to index $i = N$. For example, if the conductance spectra is to be evaluated in the frequency range 25 kHz to 30 kHz, then f_{start} would be 25 kHz and f_{end} would be 30 kHz. For any intermediate frequency f_{int}, the corresponding index $i = (N-1)\times\frac{f_{int}-f_{start}}{f_{end}-f_{start}}+1$. The corresponding values of conductance for baseline (uncorroded) state (0) and corroded state (1) are denoted as G_i^0 and G_i^1, respectively. To evaluate the RMSD (%) as per Eq. (1), the values of G_i^0 and G_i^1 should be evaluated for all recorded frequency values in the conductance spectra. An illustration of the method is shown in Fig. 1. For analytical and FE model of RMSD, it is necessary to determine change in thickness of the anode due to corrosion and formation of corrosion by-products. Corrosion, being an electrochemical reaction, is governed by the ideal mass-loss equation depicted by Faraday's law:

$$\Delta m = \frac{M}{Fz}\int_0^T I\,dt \tag{2}$$

where Δm is the mass loss, I is current passing through the cell (impressed current in accelerated corrosion experiment), M is molecular weight of the reactive species, T is total time duration for which current flows in the cell starting from $t = 0$, F is Faraday's constant, and z is valency of the reactive species. In our previous work [33], we established that the reduction in overall mass of the sacrificial anode is attributed to conversion of zinc to zinc oxide, and partial delamination of zinc oxide from the anode surface. The change in delamination front of a polymeric coating from zinc surface in the presence of electrolyte shows a power law dependence with time [41]:

$$a_{del} = k \times t^A \tag{3}$$

where a_{del} is the distance of the delamination front from the edge of the plate, k is the rate constant, t is the exposure time for delamination to occur, and A is the exponent in the power law. Using Eq. (3), we define a parameter termed as the non-delaminated factor Γ_d, which is the ratio of the non-delaminated thickness of zinc oxide layer h_d to the total thickness of the zinc oxide layer in absence of delamination h [33]:

$$\Gamma_d = \frac{h_d}{h} = 1 - \frac{2a_{del}}{a} + \frac{a_{del}^2}{a^2} \tag{4}$$

Using Eqs. (3) and (4), the non-delamination factor for a circular disk undergoing corrosion can be generalized as:

$$\Gamma_d = 1 - C_1 t^A + C_2 t^{2A} \tag{5}$$

where C_1 and C_2 are reaction dependent constants. Parameters A, C_1 and C_2 are empirically determined [33]. Eqs. (2) and (4) are together used to determine the variation in thickness of zinc and zinc oxide layers with increasing degree of accelerated corrosion due to externally applied impressed current.

3. Experimental setup

The sacrificial anode specimens used for the studies are disk shaped zinc anodes (Canode, Krishna Conchem Products Pvt. Ltd.) of diameter 3.6 cm and thickness 1.4 cm. Each anode was instrumented with a PZT transducer for obtaining EMI measurements. PZT transducer of dimensions 20 mm × 20 mm × 0.4 mm (SP-5H, Sparkler Ceramics Pvt. Ltd.) was attached to one of the circular faces of each anode using an instant adhesive (Fevikwik®) as shown in Fig. 2(a). For water proofing and protecting the transducer, a 3D printed ABS plastic cap was then attached (Fig. 2(b)) using Bondtite™ Fast & Clear, a two-component epoxy adhesive which was allowed to cure for 1 h. The 3D cap encloses the PZT transducer, creating an air pocket around the PZT transducer that protects it from water, mechanical impacts and stresses inside the mortar and concrete embedding. Two samples of anodes with 3D cap encapsulation were fabricated and embedded in hexagonal shaped conductive mortar (resistivity: 12 500 Ω cm, shown in Fig. 2(c)). One of these samples was directly used for the accelerated corrosion experiment, while the other sample was attached to steel rebars cast in a concrete block of dimensions 150 mm × 150 mm × 150 mm (illustration shown in Fig. 3), and then subjected to accelerated corrosion.

The samples are first tested for functionality by analyzing the EMI spectra of the PZT transducer which is measured using a precision LCR meter (Agilent E4980 A). The LCR meter is connected to a host computer via USB, and controlled using a custom-developed software designed with LabVIEW for data acquisition. In order to study the impact of accelerated corrosion on the EMI spectra, we first need to choose an appropriate resonance mode of the structure for further analysis. Fig. 4(a) shows conductance spectra on experimental specimens tested under three conditions: (i) 'Not embedded' (i.e. freely suspended, without embedding in conductive mortar and concrete), (ii) 'Mortar' (i.e. after embedding in conductive mortar), and (iii) 'Concrete block' (i.e. the anode is first embedded in conductive mortar, and then inside an RC block as shown in Fig. 3. The mortar and RC block samples were not immersed in electrolyte during these measurements. The 'Not embedded' i.e. freely suspended anode shows two distinct resonance peaks in the frequency range 20 kHz to 80 kHz at 42.75 kHz and 61.04 kHz with

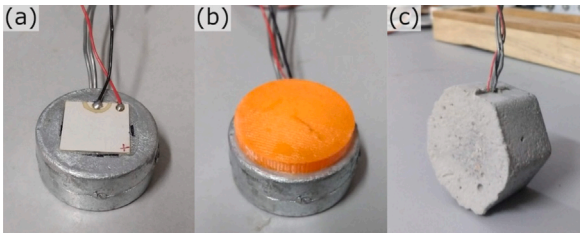

Fig. 2. (a) PZT transducer attached to a cylindrical zinc sacrificial anode. (b) 3D printed ABS plastic cap attached for water proofing of the PZT transducer. (c) The assembly in panel (b) embedded in conductive mortar. The components have following dimensions: sacrificial anode: 3.6 cm and thickness 1.4 cm; PZT transducer: 20 mm × 20 mm × 0.4 mm; hexagonal shaped conductive mortar: 28.9 mm side and 31.5 mm height.

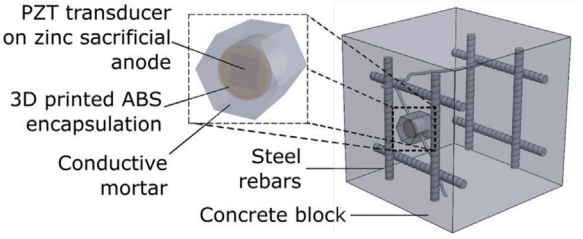

Fig. 3. 3D illustration of experimental specimen shown in Fig. 2(c) embedded in conductive mortar, which is then connected to rebars inside an RC block of dimensions: 150 mm × 150 mm × 150 mm.

quality factors of 75 and 88 respectively. As expected, the resonance peaks of the embedded anodes at 26.19 kHz and 56.54 kHz in 'Mortar' and 'Concrete block' are heavily damped with quality factors of 60 and 28 respectively (Fig. 4(b)). Further, the impact of immersion of these samples in electrolyte solution needs to be studied, for performing accelerated corrosion experiments. The 'Mortar' and 'Concrete block' specimens were immersed in electrolyte solution (9% NaCl) and kept undisturbed for more than 24 h for wetting. The EMI spectra were measured again in the same frequency range. Distinct resonances are observed at 27.45 kHz for anode embedded in mortar and 57.35 kHz for the anode embedded in concrete block. These modes are evaluated for further analysis as described in subsequent sections. We observe further damping of the resonance peaks in the EMI spectrum due to immersion in the liquid electrolyte with quality factor reducing to 20 in 'Mortar' and 6.9 in 'Concrete block' (Fig. 4(c)). While there is another resonance beyond 60 kHz for the anode embedded in mortar, it has lower quality factor of 2.7 and is therefore not considered for further analysis.

4. Simulation setup

To study the corrosion induced variation in RMSD, the zinc anode instrumented with PZT transducer embedded in mortar was modeled in a commercially available FE software (COMSOL Multiphysics). The presence of surrounding medium (9% NaCl solution or concrete) introduces damping to the system (Zn+PZT+conductive mortar). PML was used to introduce this damping in the FE model. In order to realistically model the evolution of the experimental structure due to corrosion, it would be necessary to take into account all losses in the system, and the dissipative acoustic energy radiating outward from the system. PML is an artificial domain that emulates an open and non-reflecting infinite domain, while accounting for internal losses due to damping in the system as support/anchor losses to the medium. If PML were not used, it would be necessary to assign damping coefficients to each and every material in the FE model, including ill-defined boundaries of the zinc and zinc oxide domains that vary non-uniformly due to corrosion. This approach is computationally impractical, and therefore the PML

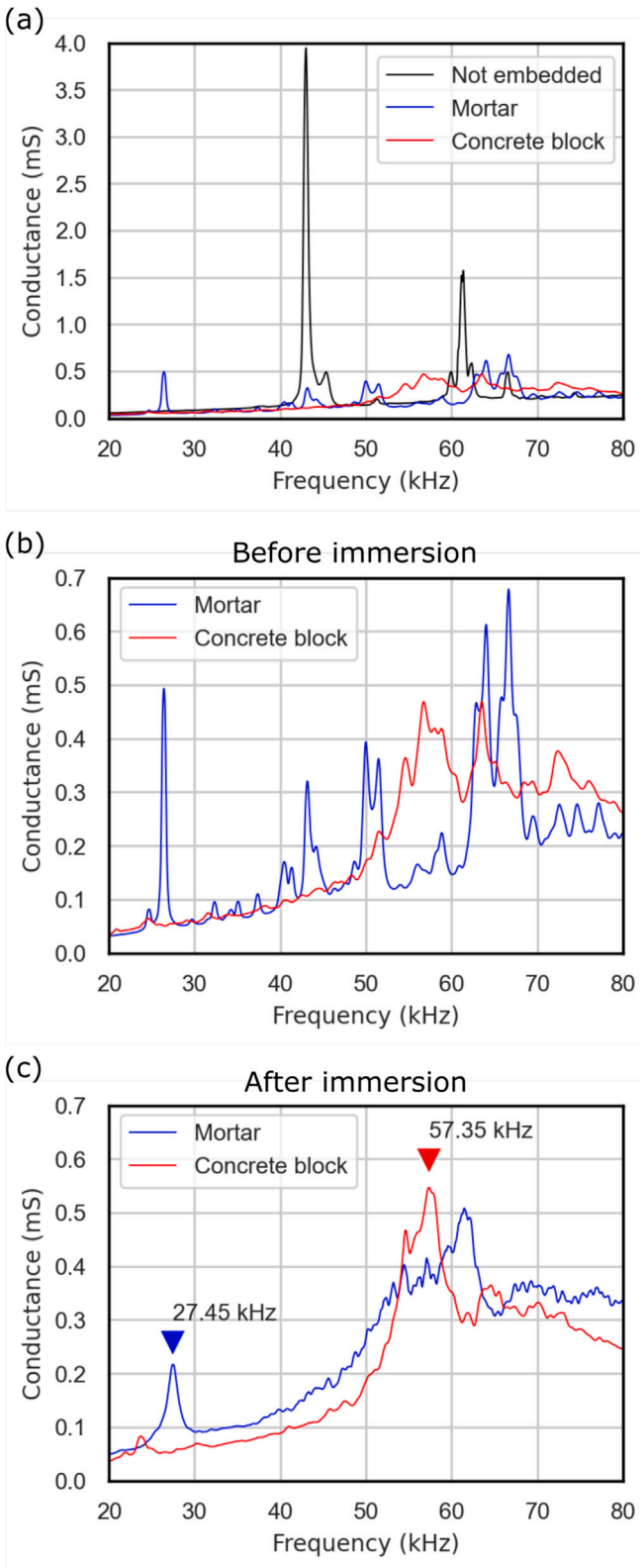

Fig. 4. (a) Conductance spectra of PZT transducer attached to the sacrificial anode with 3D printed cap, tested for three conditions: (i) 'Not embedded' (i.e. freely suspended), (ii) 'Mortar' (i.e. after embedding in conductive mortar), and (iii) 'Concrete block' (i.e. the anode is first embedded in conductive mortar, and then inside an RC block as shown in Fig. 3. The decrease in quality factor in the electromechanical resonances due to embedding of the smart anode in mortar and concrete block are evident. (b) Zoomed-in view of conductance spectra from panel (a), for 'Mortar' and 'Concrete block' specimens, prior to immersion in electrolytic solution. (c) Effect of immersion of 'Mortar' and 'Concrete block' specimens in an electrolytic solution for accelerated corrosion, showing distinct resonance peaks at 27.45 kHz and 57.35 kHz, respectively.

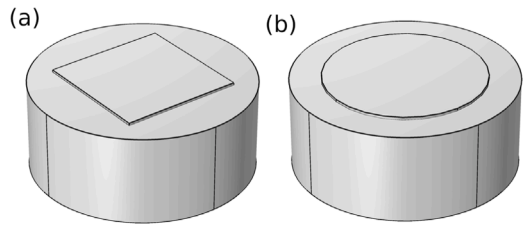

Fig. 5. (a) 3D model of 20 mm × 20 mm × 0.4 mm PZT transducer affixed on sacrificial anode disk. (b) Equivalent model showing the equivalent circular PZT transducer with radius 13 mm.

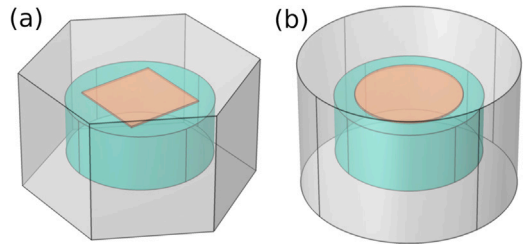

Fig. 6. (a) 3D model of hexagonal shaped mortar specimen with dimensions: 28.9 mm side and 31.5 mm height. The anode instrumented with PZT (Fig. 5(a)) is embedded in the mortar. (b) Equivalent circular model with dimensions: 26.6 mm radius and 31.5 mm height. The anode with equivalent circular PZT transducer (Fig. 5(b)) is embedded in the mortar.

approximation is widely used in axisymmetric framework for modeling acoustic losses in electro-mechanical resonators [42].

The conductance is the real part of the admittance solution computed using the *frequency domain* study. To reduce the computational complexity (time and memory of the analysis), the frequency domain study was conducted on a 2D axisymmetric model. The equivalent circular models of the hexagonal shaped sample (Fig. 2(c)) are derived following the method described in our recent work [33,43], summarized below.

For the 2D axisymmetric analysis, the square shaped PZT transducer has to be modeled as an equivalent circular shaped PZT transducer with radius a_T [33]:

$$a_T = L\frac{\beta_T}{\pi} \tag{6}$$

where L denotes the edge length of the square PZT transducer, β_T is the dimensionless frequency parameter obtained by solving the characteristic equation $\beta_T J_0(\beta_T) - (1-\nu_T)J_1(\beta_T) = 0$, where J_0 and J_1 are the Bessel functions of first kind of order 0 and 1, respectively [44], and ν_T denotes the Poisson's ratio of the transducer material (PZT). The PZT transducer used in our experiment was square-shaped with edge length 20 mm, that therefore corresponds to an equivalent circular PZT transducer with radius 13 mm [33], shown in Fig. 5.

The sacrificial anode with PZT transducer encapsulated in a ABS cap was embedded in a hexagonal cross-section shaped conductive mortar as shown in Fig. 2(c). For representing in 2D axisymmetric model, the structure was modeled as a plate, and the fundamental transverse vibration equation for the hexagonal plate equated to vibration mode of an equivalent circular plate. For a hexagonal thin plate undergoing transverse mode (mode (0, 1)) of vibration with 'free edge' boundary conditions, the fundamental frequency is expressed as [45]:

$$\omega = \lambda\frac{\pi^2}{a^2}\sqrt{\frac{D}{\rho h}} \tag{7}$$

where λ is the dimensionless frequency parameter, $\frac{a}{2}$ is the side of the hexagon, D is the flexural rigidity of the plate given by $D = \frac{Eh^3}{12(1-\nu^2)}$, ρ is the density of the material and h is the thickness of the plate.

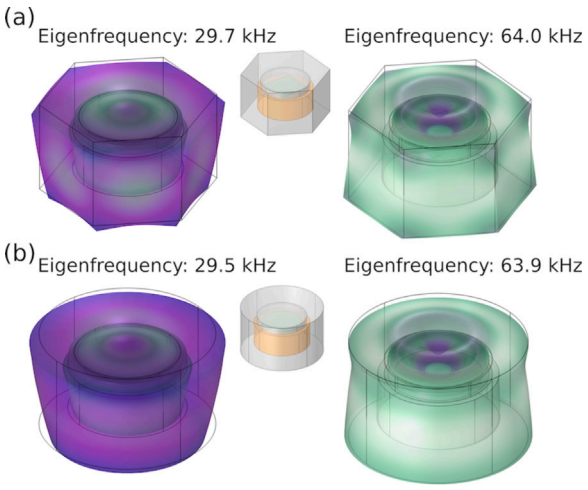

Fig. 7. (a) Natural resonance frequencies of transverse modes of vibration for structure shown in Fig. 6(a) are 29.7 kHz and 64.0 kHz. (b) Natural resonance frequencies of transverse modes of vibration for the equivalent circular disk shaped structure shown in Fig. 6(b) are 29.5 kHz and 63.9 kHz.

Similarly, for a circular thin plate, the fundamental frequency of the same transverse mode is expressed as [46]:

$$\omega = \beta\frac{1}{r_{eq}^2}\sqrt{\frac{D}{\rho h}} \tag{8}$$

where β is the dimensionless frequency parameter obtained from solving the characteristic equation, r_{eq} is the radius of the equivalent circular model. The radius of the equivalent circular model, obtained by equating Eqs. (7) and (8), is expressed as:

$$r_{eq} = \frac{a}{\pi}\sqrt{\frac{\beta}{\lambda}} \tag{9}$$

The equivalent circular model was used for performing 2D axisymmetric FE analysis. The presence of surrounding medium around the conductive mortar introduces damping into the system which can be captured using the PML layer around the model. The minimum thickness of the PML layer is equal to one wavelength of sound wave propagating in the PML medium. It is strongly recommended to use mapped meshing in the PML domains so as to not cause poor mesh element quality. A minimum of ten elements (in the radial direction) are required in the PML layer to achieve convergence. For all other regions, extremely fine mesh setting was used.

5. Simulation results

The dimensionless parameter λ for a hexagonal plate undergoing transverse vibration is 4.3238 [45], while that of the circular plate β is 9.003 [46]. Fig. 6 shows the 3D model of the hexagonal specimen (28.9 mm side and 31.5 mm height) and the equivalent circular model (26.6 mm radius and 31.5 mm height). Fig. 7 shows the resonant modes of the structures obtained using eigenfrequency FE analysis (undamped) in COMSOL Multiphysics, corresponding to the resonance frequencies in vicinity of the peaks observed in Fig. 4(b). The equivalence of the two structures was validated by observing that resonance frequencies for the two modes of interest for the actual geometry of the specimen (Fig. 7(a): 29.7 kHz and 64.0 kHz) match closely with those of the equivalent circular model: (Fig. 7(b): 29.5 kHz and 63.9 kHz) i.e. amounting to <0.7% error. Note that the FE results for eigenfrequencies do not match exactly with the experimentally measured values reported in Fig. 4(b), as the material properties predefined in COMSOL Multiphysics library used for performing the simulations may differ slightly from those of the experimental specimens.

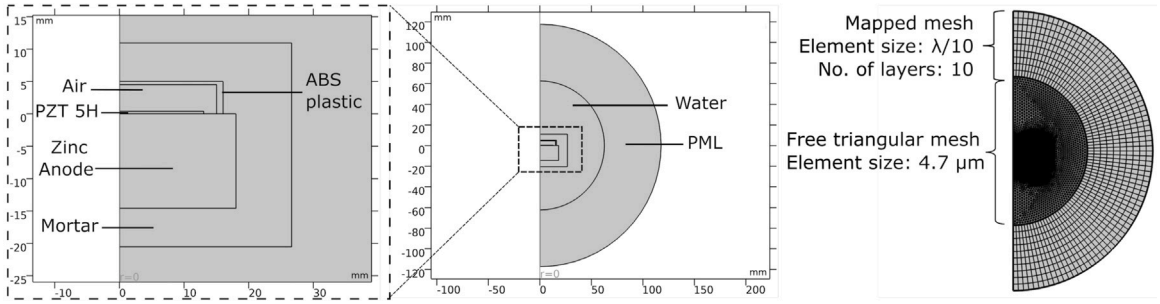

Fig. 8. 2D axisymmetric model for sacrificial anode embedded in mortar surrounded by water, PML and zoomed-in view showing the arrangement of transducer inside the 3D plastic cap. Also shown are the meshing parameters used in the model for simulations, with mapped mesh element size $\lambda/10 = 5.5$ mm.

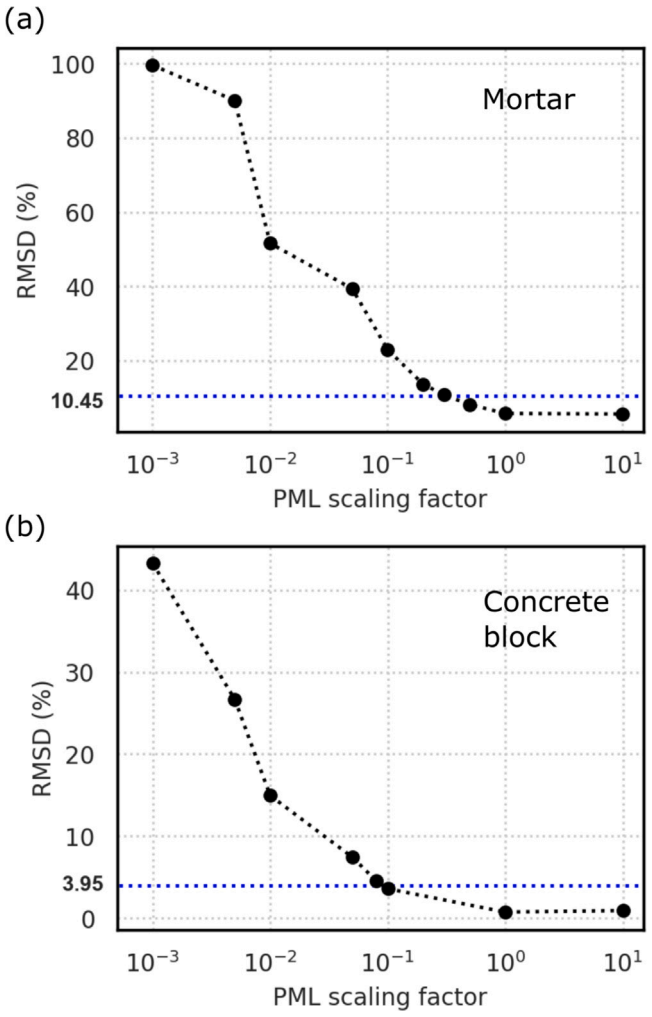

Fig. 9. Variation of RMSD (corresponding to application of 0.47 A current for 30 min with 9% NaCl solution) with the PML scaling factor for: (a) 'Mortar', and (b) 'Concrete block' specimens. The optimal PML scaling factor is obtained by equating the RMSD value obtained from FE simulations to experimental results. RMSD and PML scaling factor for 'Mortar': 10.45 and 0.28, respectively. RMSD and PML scaling factor for 'Concrete block': 3.95 and 0.09, respectively.

Fig. 8 shows a schematic illustration of the setup for the anode in conductive mortar specimen immersed in water (i.e. NaCl solution). For the case of water as the surrounding medium (i.e. specimen 'Mortar' as described in Section 3), the radius of the spherical layer was taken as 62.5 mm, since it matched the volume of NaCl solution used in the experiment. The thickness of PML layer was obtained as 55 mm, the mapped mesh element size was correspondingly set to 5.5 mm. In case of concrete as the surrounding medium (i.e. specimen 'Concrete block' as described in Section 3), the radius of the spherical layer is taken as 93.06 mm such that it matches the volume of the concrete cube used in the experiment. The energy loss in the system undergoing vibrations due to damping can be adjusted using the scaling factor of PML layer properties. Fig. 9 shows the variation of RMSD for a range of PML scaling factor varying from 10^{-3} to 10^{1}. The RMSD is obtained for conductance spectrum obtained through FE simulation for frequency span of 10 kHz around the resonance frequency (i.e. 22.45 kHz to 32.45 kHz for 27.45 kHz mode in 'Mortar' and 52.35 kHz to 62.35 kHz for 57.35 kHz mode in 'Concrete block' specimen), for a geometry corresponding to application of 0.47 A current for 30 min with 9% NaCl solution i.e. thickness of Zn and ZnO layers set to 14.585 mm and 0.024 mm, respectively in the FE model. The optimal PML scaling factor is obtained by equating the RMSD value at 30 min obtained from FE simulations to experimental results (RMSD for 'Mortar': 10.45, 'Concrete block': 3.95). The corresponding PML scaling factors are 0.28 for 'Mortar' and 0.09 for 'Concrete block'. The experimental results are described in the next section.

6. Experimental results

The experimental setup for accelerated corrosion by means of applied impressed current consisted of an electrolytic cell with a set of two electrodes submerged in an electrolyte. We used a copper tube as cathode and 9% NaCl solution as electrolyte as previously described. The copper electrode was connected to negative terminal of a constant current source (Aplab LQ6324T) while positive terminal of the current source was connected to the zinc sacrificial anode assembly. The constant current source supplied current of magnitude 0.47 A, for inducing large amount of accelerated corrosion in reasonably short time [47–49]. Note that the applied current magnitude (0.47 A) is much higher than naturally observed current densities during corrosion of rebars. Although impressed current based accelerated corrosion results in difference in the morphology of corroded surface and corrosion by-products as compared to natural corrosion, it is a commonly accepted laboratory technique to induce accelerated corrosion to understand and study the progression of corrosion, and therefore was used in this study. However, the discussion of this aspect of accelerated corrosion as compared to natural corrosion is limited to rebars in literature [50–52], and no such studies are reported for zinc sacrificial anodes. After every 30 min interval, the current source was turned off and impedance of the PZT transducer was recorded with the LCR meter, without disturbing the mechanical arrangement of the apparatus. Fig. 10 shows photographs of the experimental setups for the 'Mortar' and 'Concrete block' samples, and the corresponding EMI spectra obtained every 30 min for a total duration of 120 min. The change in color of the electrolyte with increasing time is a visual indicator of progression of corrosion [47], as shown in Fig. 11. We observe marked difference in the conductance spectra for the 'Mortar' and 'Concrete block' samples (Figs. 10(b) and (d)) with progressing time for which impressed current

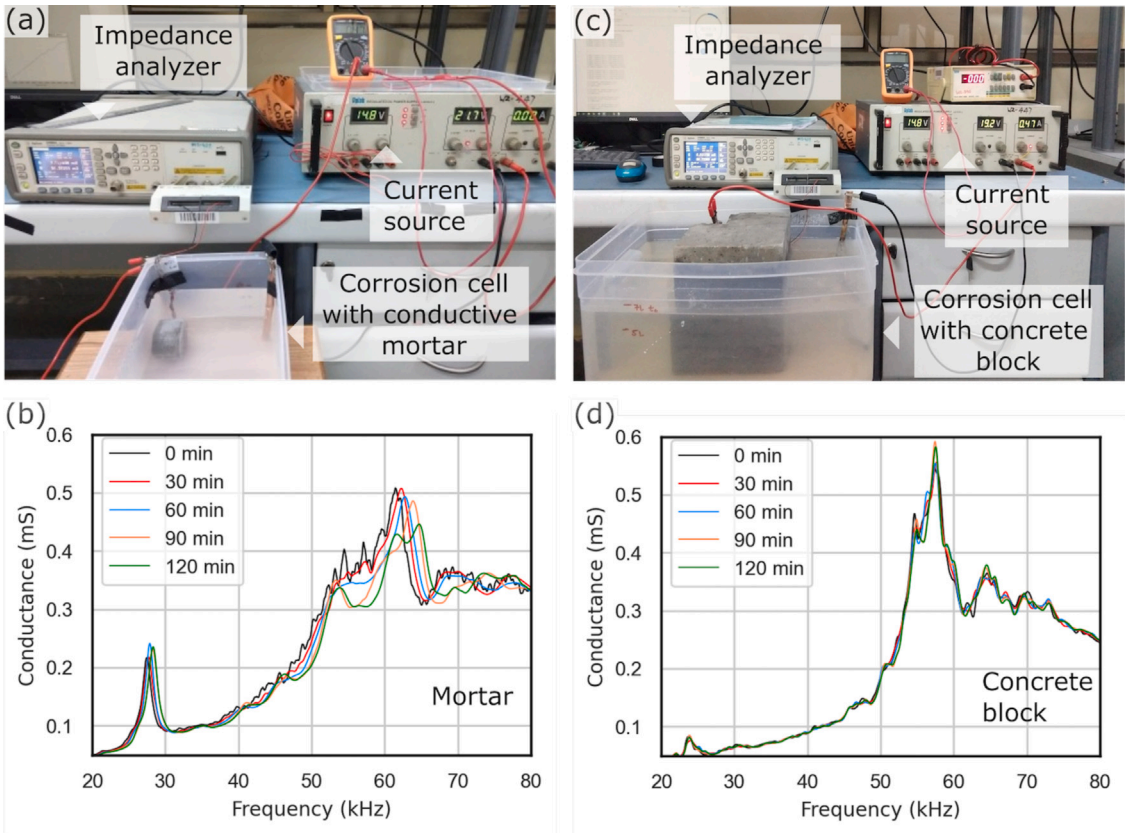

Fig. 10. Accelerated corrosion apparatus and experimental results for conductance spectra obtained for (a) & (b) 'Mortar' specimen, and (c) & (d) 'Concrete block' specimen, respectively.

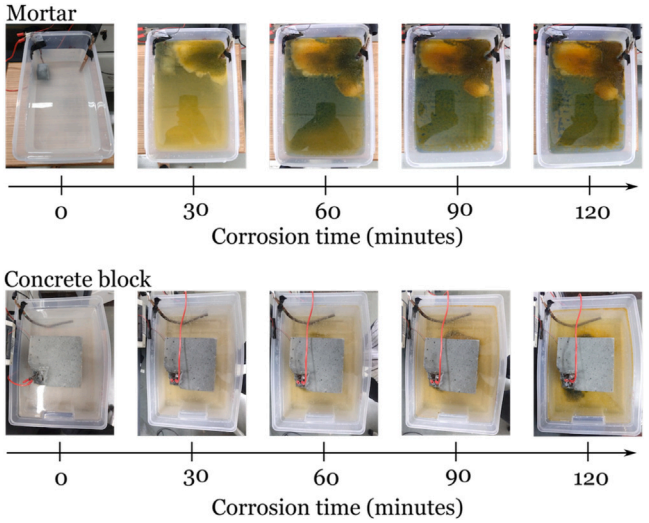

Fig. 11. Progressive change in color of electrolyte due to corrosion of the sacrificial anode embedded in (a) Mortar, and (b) Concrete block.

is applied, indicating change in mechanical impedance due to corrosion. The RMSD was computed in 10 kHz frequency span around the resonance frequency i.e. 27.45 kHz in 'Mortar' and 57.35 kHz in 'Concrete block' (Figs. 12(a) and (c)). The variation of RMSD values with time, calculated for the experimental data, are shown in Figs. 12(b) and (d). The non-linearity in the trend was attributed to the delamination of corrosion by-product, and was corroborated with FE simulation results. The non-linearity was more pronounced for the sensor embedded in the concrete block. The parameters C_1, C_2 and A were estimated for both samples using MATLAB Curve Fitting Toolbox to fit the experimental data, and the non-delamination factors thus obtained are:

$$\Gamma_d(t) = \begin{cases} 1 - 0.040t^{0.895} + 0.014t^{2\times0.895} & \text{Mortar} \\ 1 - 0.242t^{0.825} + 0.026t^{2\times0.825} & \text{Concrete block} \end{cases}$$

Table 2 shows the thicknesses of the Zn and ZnO layers estimated with the corresponding Γ_d values for both samples. These values are plugged into the FE model with PML, and the RMSD values thus obtained show excellent agreement with experimental data (Figs. 12(b) and (d)). Thus, the analytical and FE models allow estimation of state of health of the sacrificial anode through non-destructive EMI testing. Despite the damping introduced by the mortar and concrete cover, the technique is able to discern corrosion of the sacrificial anode through studying variation in the RMSD. The advantage of this system is that it can be adapted for any arbitrary geometry (shape) of the sacrificial anode, by studying the corresponding resonant modes. Because of the modest profile of the PZT transducer, it can be easily installed using already available methods used for installation of sacrificial anodes at key locations in civil infrastructure. It should however be noted that the extent of corrosion of the sacrificial anode as measured by PZT transducer attached to the anode is representative of corrosion severity of the reinforcement bars in vicinity of the anode to which it is connected, i.e. this technique provides a glimpse of corrosivity of the local environment of the anode. Nevertheless, the technology could be very useful in estimating remaining service life of the sacrificial anodes and structure under protection, and enables condition based maintenance instead of preventive or time-based maintenance of infrastructure instrumented with sacrificial anodes.

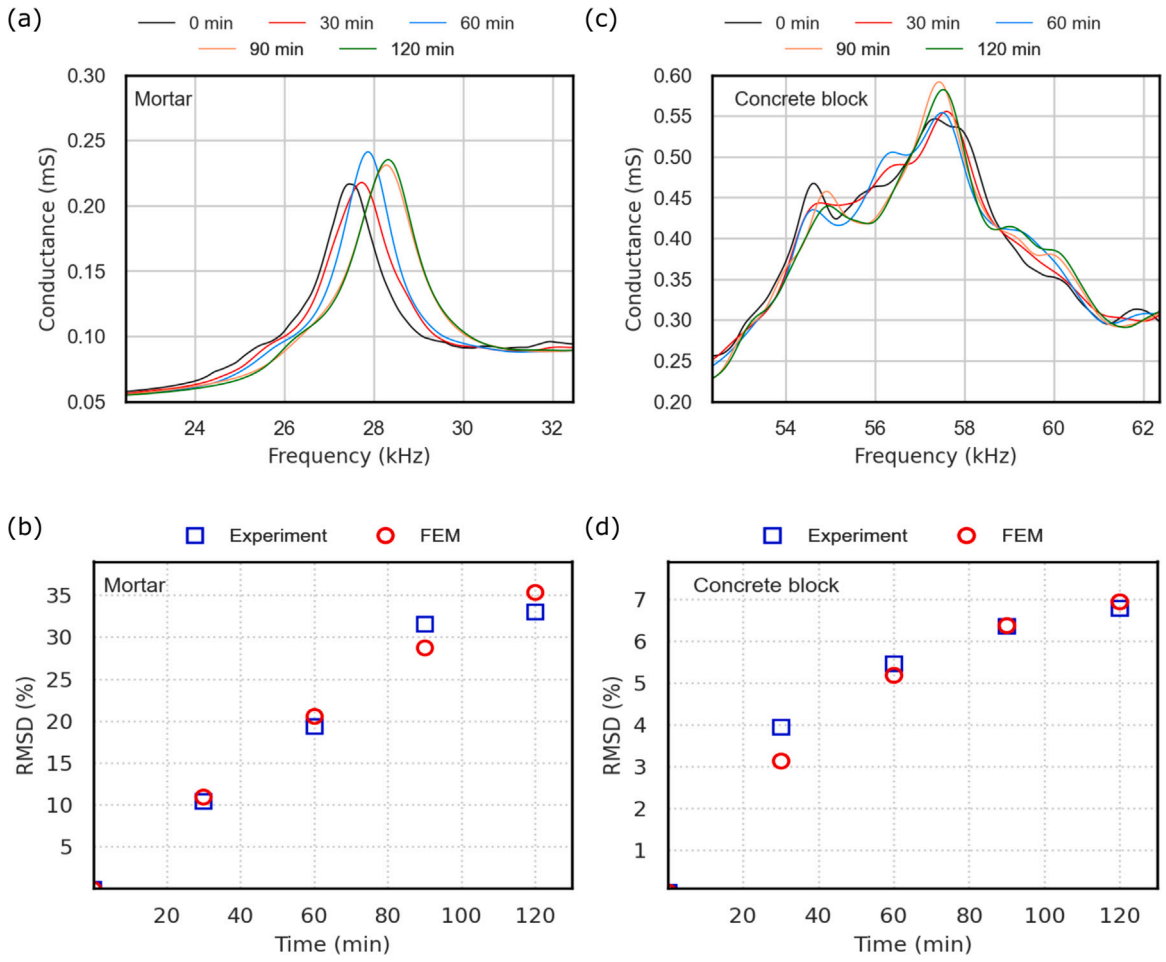

Fig. 12. Experimentally measured variation of the conductance signature in 10 kHz frequency span for: (a) 27.45 kHz mode in 'Mortar' specimen, and (b) comparison of experimentally measured RMSD with solution obtained from FE simulation for 'Mortar' specimen. Corresponding results for 'Concrete block' specimen, for 57.35 kHz mode are shown in panels (c) & (d).

Table 2
Thickness of Zn and ZnO layers estimated for anodes in 'Mortar' and 'Concrete block' samples.

Time [min]	Mortar		Concrete block	
	Zn [mm]	ZnO [mm]	Zn [mm]	ZnO [mm]
0	14.600	0	14.600	0
30	14.5850	0.0229	14.5850	0.0205
60	14.5699	0.0445	14.5699	0.0369
90	14.5549	0.0645	14.5549	0.0504
120	14.5398	0.0826	14.5398	0.0615

7. Discussion

The primary advantage of the EMI technique over conventional methods is that the degradation of the sacrificial anode embedded in the concrete structure can be deterministically and non-destructively assessed in real-time. This technique is cost-effective and can be equipped with impedance analyzer semiconductor ICs (e.g. Analog Devices AD5933) and remote monitoring capabilities to realize simplified and compact structural health monitoring systems. A limitation of this method is that the electro-mechanical resonances of higher order modes showed significant damping upon embedding in mortar and concrete, and therefore could not be used in conjunction with the inverse graphical technique presented in our previous work [43]. This necessitates the estimation of Γ_d factor empirically. Since this factor varies for each anode depending on the environment under which the anode operates and variations in manufacturing, the method presented in this work therefore requires a calibration method to be developed suitable for in-field deployment. Since every specimen of smart anode embedded in concrete will have varying damping conditions due to the heterogeneity of its surroundings and dimensions of the specimen, the baseline EMI value has to be acquired for each such specimen at the time of installation, in order to calculate RMSD at subsequent times upon progression of corrosion. Therefore, for an unknown specimen without reference data collected during installation, the EMI technique described in this manuscript cannot be applied. Nevertheless, the EMI method shown in this work would be useful as a real-time structural health monitoring (SHM) technique, and any deviations in RMSD could be used to make decisions about deploying suitable NDT techniques such as pulsed eddy current (PEC), to estimate the extent of corrosion. We have recently shown preliminary results on comparative analysis of EMI and PEC [53], to further highlight the utility of EMI based sacrificial anode monitoring technique.

8. Conclusion and future work

We have demonstrated feasibility of using PZT-based EMI method to monitor incipient corrosion in zinc sacrificial anodes. The performance of this system is evaluated with the anode embedded in conductive mortar and in an RC block. We study the performance of the method using RMSD of the conductance spectra as a metric to analyze change in state-of-health of the anode. The RMSD is observed to be highly sensitive to corrosion of the sacrificial anode, despite the large damping

of the electro-mechanical resonance introduced by the mortar and concrete. For example, application of 0.47 A impressed current for 120 min in 9% NaCl solution results in RMSD of 6.78% for anode embedded in concrete block, despite reduction of the quality factor of the transverse mode of vibration from 88 for freely suspended anode vibrating in air, to 6.9 for the anode in mortar embedded in reinforced concrete block. Further, analytical and FE models were developed for validating the experimental results obtained using impressed current based accelerated corrosion setup. The experimental results and simulations show excellent agreement with each other. The non-linearity in the RMSD trend with increasing time of application of impressed current is adequately explained by the delamination dynamics captured by the models. In future work, we will study the impact of anode geometry on damping of higher order modes, and optimize the structure of the anode and the packaging to improve the quality factors of the vibration modes, such that the inverse graphical technique can be applied without having to estimate Γ_d [43]. Several other factors such as temperature, concrete hydration, type of cement etc. that could affect the EMI measurements are yet to be investigated and would be undertaken in future work. In summary, the proposed system has a high potential for field deployment to detect early corrosion in sacrificial anodes embedded in concrete for protection of RC structures.

CRediT authorship contribution statement

Durgesh Tamhane: Conceptualization, Methodology, Investigation, Writing – original draft. **Jeslin Thalapil:** Conceptualization, Methodology, Investigation, Writing – original draft. **Sauvik Banerjee:** Conceptualization, Methodology, Writing – review & editing, Project administration, Funding acquisition. **Siddharth Tallur:** Conceptualization, Methodology, Writing – review & editing, Project administration, Funding acquisition.

Declaration of competing interest

The authors declare that they have no known competing financial interests or personal relationships that could have appeared to influence the work reported in this paper.

Acknowledgments

This work was supported by IMPRINT-2 A administered by Science and Engineering Research Board (SERB), Department of Science & Technology, Government of India [grant IMP/2018/001442] with additional financial support from Sanrachana Structural Strengthening Pvt. Ltd. [grant RD/0119-SSIMPQ2-001]. The authors thank Mr. Hrishikesh Belatikar at IIT Bombay for assistance with developing the LabVIEW based data acquisition software, and Wadhwani Electronics Lab (WEL) at IIT Bombay for providing Agilent E4980A precision LCR meter.

References

[1] J. Broomfield, Corrosion of Steel in Concrete: Understanding, Investigation and Repair, CRC Press, 2003.
[2] G. Koch, Cost of corrosion, in: Trends in Oil and Gas Corrosion Research and Technologies, Elsevier, 2017, pp. 3–30.
[3] L. Bertolini, M. Gastaldi, M. Pedeferri, E. Redaelli, Prevention of steel corrosion in concrete exposed to seawater with submerged sacrificial anodes, Corros. Sci. 44 (7) (2002) 1497–1513.
[4] S. Szabo, I. Bakos, Cathodic protection with sacrificial anodes, Corros. Rev. 24 (3–4) (2006) 231–280.
[5] R. Brousseau, B. Baldock, Laboratory study of sacrificial anodes for reinforced concrete, Corrosion 54 (03) (1998).
[6] J.-A. Jeong, W.-S. Chung, Y.-H. Kim, Electrochemical measurements of cathodic protection for reinforced concrete piles in a marine environment using embedded corrosion monitoring sensors, Met. Mater. Int. 19 (3) (2013) 445–452.
[7] C. Zhang, G.P. Panda, Q. Yan, W. Zhang, C. Vipulanandan, G. Song, Monitoring early-age hydration and setting of portland cement paste by piezoelectric transducers via electromechanical impedance method, Constr. Build. Mater. 258 (2020) 120348.
[8] Y.-F. Su, G. Han, A. Amran, T. Nantung, N. Lu, Instantaneous monitoring the early age properties of cementitious materials using PZT-based electromechanical impedance (EMI) technique, Constr. Build. Mater. 225 (2019) 340–347.
[9] P. Negi, T. Chakraborty, N. Kaur, S. Bhalla, Investigations on effectiveness of embedded PZT patches at varying orientations for monitoring concrete hydration using EMI technique, Constr. Build. Mater. 169 (2018) 489–498.
[10] S. Zhao, S. Fan, J. Yang, S. Kitipornchai, A spherical smart aggregate sensor based electro-mechanical impedance method for quantitative damage evaluation of concrete, Struct. Health Monit. 19 (5) (2020) 1560–1576.
[11] D. Ai, H. Zhu, H. Luo, Sensitivity of embedded active PZT sensor for concrete structural impact damage detection, Constr. Build. Mater. 111 (2016) 348–357.
[12] T.J. Saravanan, K. Balamonica, C.B. Priya, A.L. Reddy, N. Gopalakrishnan, Comparative performance of various smart aggregates during strength gain and damage states of concrete, Smart Mater. Struct. 24 (8) (2015) 085016.
[13] A. Narayanan, K.V. Subramaniam, Sensing of damage and substrate stress in concrete using electro-mechanical impedance measurements of bonded PZT patches, Smart Mater. Struct. 25 (9) (2016) 095011.
[14] J. Ahmadi, M.H. Feirahi, S. Farahmand-Tabar, A.H.K. Fard, A novel approach for non-destructive EMI-based corrosion monitoring of concrete-embedded reinforcements using multi-orientation piezoelectric sensors, Constr. Build. Mater. 273 (2021) 121689.
[15] T. Bansal, V. Talakokula, Deterioration of structural parameters due to corrosion in prestressed concrete identified by smart probe-based piezo sensor, Eng. Res. Express 3 (1) (2021) 015011.
[16] W. Shi, Y. Chen, P. Liu, D. Xu, Corrosion investigation of reinforced concrete based on piezoelectric smart materials, Materials 12 (3) (2019) 519.
[17] G.E. Simmers Jr., Impedance-Based Structural Health Monitoring to Detect Corrosion (Ph.D. thesis), Virginia Tech, 2005.
[18] S. Park, B.L. Grisso, D.J. Inman, C.-B. Yun, MFC-Based structural health monitoring using a miniaturized impedance measuring chip for corrosion detection, Res. Nondestruct. Eval. 18 (2) (2007) 139–150.
[19] V. Bedekar, D. Inman, S. Priya, Detection of corrosion using impedance spectroscopy, Ferroelectr. Lett. Sect. 35 (1–2) (2008) 7–16.
[20] Y. Yang, B.S. Divsholi, Sub-frequency interval approach in electromechanical impedance technique for concrete structure health monitoring, Sensors 10 (12) (2010) 11644–11661.
[21] V. Talakokula, S. Bhalla, Reinforcement corrosion assessment capability of surface bonded and embedded piezo sensors for reinforced concrete structures, J. Intell. Mater. Syst. Struct. 26 (17) (2015) 2304–2313.
[22] V. Talakokula, S. Bhalla, R. Ball, C. Bowen, G. Pesce, R. Kurchania, B. Bhattacharjee, A. Gupta, K. Paine, Diagnosis of carbonation induced corrosion initiation and progression in reinforced concrete structures using piezo-impedance transducers, Sensors Actuators A 242 (2016) 79–91.
[23] W.S. Na, Possibility of detecting wall thickness loss using a PZT based structural health monitoring method for metal based pipeline facilities, NDT E Int. 88 (2017) 42–50.
[24] W. Li, T. Liu, D. Zou, J. Wang, T.-H. Yi, PZT Based smart corrosion coupon using electromechanical impedance, Mech. Syst. Signal Process. 129 (2019) 455–469.
[25] P. Astuti, R. Rafdinal, H. Hamada, Y. Sagawa, D. Yamamoto, K. Kamarulzaman, Effectiveness of rusted and non-rusted reinforcing bar protected by sacrificial anode cathodic protection in repaired patch concrete, in: IOP Conference Series: Earth and Environmental Science, Vol. 366, IOP Publishing, 2019, 012013.
[26] U.M. Angst, A critical review of the science and engineering of cathodic protection of steel in soil and concrete, Corrosion 75 (12) (2019) 1420–1433.
[27] A. Farooq, M. Hamza, Q. Ahmed, K.M. Deen, Evaluating the performance of zinc and aluminum sacrificial anodes in artificial seawater, Electrochim. Acta 314 (2019) 135–141.
[28] G. Sergi, Ten-year results of galvanic sacrificial anodes in steel reinforced concrete, Mater. Corros. 62 (2) (2011) 98–104.
[29] C. Liang, F.P. Sun, C.A. Rogers, Electromechanical impedance modeling of active material systems, in: Smart Structures and Materials 1994: Mathematics and Control in Smart Structures, Vol. 2192, International Society for Optics and Photonics, 1994, pp. 232–253.
[30] C.K. Soh, S. Bhalla, Calibration of piezo-impedance transducers for strength prediction and damage assessment of concrete, Smart Mater. Struct. 14 (4) (2005) 671.
[31] A.S.K. Naidu, S. Bhalla, C.-K. Soh, Incipient damage localization with smart piezoelectric transducers using high-frequency actuation, in: Smart Structures, Devices, and Systems, Vol. 4935, International Society for Optics and Photonics, 2002, pp. 473–483.
[32] A.S.K. Naidu, S. Bhalla, Damage detection in concrete structures with smart piezoceramic transducers, in: Smart Materials, Structures, and Systems, Vol. 5062, International Society for Optics and Photonics, 2003, pp. 684–690.
[33] D. Tamhane, J. Thalapil, S. Banerjee, S. Tallur, Smart cathodic protection system for real-time quantitative assessment of corrosion of sacrificial anode based on electro-mechanical impedance (EMI), IEEE Access 9 (2021) 12230–12240, http://dx.doi.org/10.1109/ACCESS.2021.3051953.
[34] S. Banerji, D. Fernández, J. Madrenas, Characterization of CMOS-MEMS resonant pressure sensors, IEEE Sens. J. 17 (20) (2017) 6653–6661, http://dx.doi.org/10.1109/JSEN.2017.2747140.

[35] A. Kourani, R. Lu, S. Gong, A wideband oscillator exploiting multiple resonances in lithium niobate MEMS resonator, IEEE Trans. Ultrason. Ferroelectr. Freq. Control 67 (9) (2020) 1854–1866, http://dx.doi.org/10.1109/TUFFC.2020.2989623.
[36] G. Pillai, A.A. Zope, J.M.-L. Tsai, S.-S. Li, Design and optimization of SHF composite FBAR resonators, IEEE Trans. Ultrason. Ferroelectr. Freq. Control 64 (12) (2017) 1864–1873, http://dx.doi.org/10.1109/TUFFC.2017.2759811.
[37] V. Giurgiutiu, Structural Health Monitoring: With Piezoelectric Wafer Active Sensors, Elsevier, 2007.
[38] R. Tawie, H.-K. Lee, Monitoring the strength development in concrete by EMI sensing technique, Constr. Build. Mater. 24 (9) (2010) 1746–1753.
[39] E. Ghafari, Y. Yuan, C. Wu, T. Nantung, N. Lu, Evaluation the compressive strength of the cement paste blended with supplementary cementitious materials using a piezoelectric-based sensor, Constr. Build. Mater. 171 (2018) 504–510.
[40] S. Bhalla, P.A. Vittal, M. Veljkovic, Piezo-impedance transducers for residual fatigue life assessment of bolted steel joints, Struct. Health Monit. 11 (6) (2012) 733–750.
[41] W. Fürbeth, M. Stratmann, The delamination of polymeric coatings from electrogalvanized steel–A mechanistic approach.: Part 3: delamination kinetics and influence of CO_2, Corros. Sci. 43 (2) (2001) 243–254.
[42] D.S. Bindel, S. Govindjee, Elastic PMLs for resonator anchor loss simulation, Internat. J. Numer. Methods Engrg. 64 (6) (2005) 789–818.
[43] J. Thalapil, D. Tamhane, S. Banerjee, S. Tallur, Vibration-based inverse graphical technique for thickness estimation of bulk acoustic wave (BAW) resonators: Application for corrosion monitoring of sacrificial anodes, Smart Mater. Struct. 30 (3) (2021) 055015.
[44] V. Giurgiutiu, Structural Health Monitoring with Piezoelectric Wafer Active Sensors, second ed., Academic Press, 2014.
[45] K.M. Liew, K.Y. Lam, A set of orthogonal plate functions for flexural vibration of regular polygonal plates, J. Vib. Acoust. (ISSN: 1048-9002) 113 (2) (1991) 182–186, http://dx.doi.org/10.1115/1.2930167.
[46] A. Leissa, Vibration of Plates, NASA Report No. SP-160, SP-160, 1969.
[47] R.C. Sriramadasu, Y. Lu, S. Banerjee, Identification of incipient pitting corrosion in reinforced concrete structures using guided waves and piezoelectric wafer transducers, Struct. Health Monit. 18 (1) (2019) 164–171.
[48] T.A. El Maaddawy, K.A. Soudki, Effectiveness of impressed current technique to simulate corrosion of steel reinforcement in concrete, J. Mater. Civ. Eng. 15 (1) (2003) 41–47.
[49] H.-S. Lee, T. Noguchi, F. Tomosawa, Evaluation of the bond properties between concrete and reinforcement as a function of the degree of reinforcement corrosion, Cem. Concr. Res. 32 (8) (2002) 1313–1318.
[50] J. Wang, Z. Wang, W. Ke, Characterisation of rust formed on carbon steel after exposure to open atmosphere in qinghai salt lake region, Corros. Eng. Sci. Technol. 47 (2) (2012) 125–130.
[51] S. Hong, G. Shi, F. Zheng, M. Liu, D. Hou, B. Dong, Characterization of the corrosion profiles of reinforcement with different impressed current densities by X-ray micro-computed tomography, Cem. Concr. Compos. 109 (2020) 103583.
[52] W. Zhang, J. Chen, X. Luo, Effects of impressed current density on corrosion induced cracking of concrete cover, Constr. Build. Mater. 204 (2019) 213–223.
[53] D. Tamhane, S. Banerjee, S. Tallur, Monitoring corrosion in sacrificial anodes with pulsed eddy current and electromechanical impedance: A comparative analysis, IEEE Sens. J. (2022).